Partitioning Regulatory Mechanisms of Within-Host Malaria Dynamics Using the Effective Propagation Number

C. J. E. Metcalf, *et al.*

Science **333**, 984 (2011);
DOI: 10.1126/science.1204588

Partitioning Regulatory Mechanisms of Within-Host Malaria Dynamics Using the Effective Propagation Number

C. J. E. Metcalf,[1]* A. L. Graham,[2] S. Huijben,[3] V. C. Barclay,[3] G. H. Long,[4] B. T. Grenfell,[2,5] A. F. Read,[3,5] O. N. Bjørnstad[3,5]

Immune clearance and resource limitation (via red blood cell depletion) shape the peaks and troughs of malaria parasitemia, which in turn affect disease severity and transmission. Quantitatively partitioning the relative roles of these effects through time is challenging. Using data from rodent malaria, we estimated the effective propagation number, which reflects the relative importance of contrasting within-host control mechanisms through time and is sensitive to the inoculating parasite dose. Our analysis showed that the capacity of innate responses to restrict initial parasite growth saturates with parasite dose and that experimentally enhanced innate immunity can affect parasite density indirectly via resource depletion. Such a statistical approach offers a tool to improve targeting of drugs or vaccines for human therapy by revealing the dynamics and interactions of within-host regulatory mechanisms.

In the bloodstream phase of many malaria species, including those infecting humans, infected red blood cells (RBCs) burst in synchrony, releasing merozoites that must locate and infect a new RBC rapidly or else they die (*1*). After 24 to 72 hours (depending on the *Plasmodium* species), the next generation of merozoites bursts out. The cycle repeats itself until the host dies or clears the infection (fig. S1). Clearance of infection requires various complex immunological and physiological processes, the relative roles and timing of which have proven difficult to quantify (*2*–*4*).

We propose a straightforward statistical approach to the problem. Building on the analogy between cell-to-cell propagation and host-to-host transmission (*5*), we borrow a model from between-host disease population ecology (*6*) to show how cell-to-cell transmission of malaria can be estimated using standard experimental data from rodent malaria (the modeling framework is readily extended to suitably detailed data on human malaria; see below). If I_t is the number of infected RBCs at time t, and S_t is the number of uninfected RBCs, then the expected number of infected RBCs observed at time $t+1$ will be $E[I_{t+1}] = P_{e,t}S_tI_t$, where E denotes the expectation and $P_{e,t}$ is the effective propagation number of the infection at time t. This number can be thought of as the product of merozoite burst size, contact rates between merozoites and uninfected RBCs, and invasion probability given that a contact has occurred. This quantity is analogous to the transmission coefficient in canonical models of between-host infection dynamics (*7*). The effective propagation number will vary through time as a function of variation in the availability of susceptible RBCs and efficacy of immune mechanisms. Taking the log on both sides of the relationship above, we can write

$$\log(E[I_{t+1}]) = \log(P_{e,t}) + \log(I_t) + \log(S_t) \quad (1)$$

Applying regression techniques to Eq. 1 enables estimation of $P_{e,t}$ whenever time series of I and S are available. While of critical interest in its own right, P_e is also important because of its relation to the within-host basic (R_0) and time-varying effective (R_e) reproductive ratios. For blood-phase malaria, these two dimensionless quantities are defined as the number of newly infected cells that would arise from the merozoites that burst from a single infected cell in an otherwise uninfected bloodstream, and the average number of new infected cells per infected cell in a previously infected bloodstream, respectively (*8*). From our estimates of $P_{e,t}$, we can directly quantify the effective reproductive ratio as $R_{e,t} = P_{e,t}S_t$. When $R_e > 1$, within-host parasite density will increase. When $R_e < 1$, parasite density will decrease. The maximum upper bound on R_e (and R_0) is the burst size, or number of merozoites emerging from a single infected RBC, and is attained if the invasion probability upon contact is 1 and if crowding and immune effects are absent.

A variety of immune and nonimmune factors determine the magnitude of P_e and thus R_e. The relative importance of these factors will vary during the course of an infection because of time-dependent variation in RBC availability/susceptibility and the density of immune effectors (*9*, *10*). A standard approach to quantifying this variation is to test data against mathematical models that incorporate a series of differential equations chosen to reflect processes involving explicitly defined interacting populations of cells and effectors, as a function of time and/or pathogen titer (*3*, *5*, *11*–*18*). Focusing on P_e allows us to avoid many complex unknowns required for this approach, not least the arbitrary choice of specific functional forms for key relationships such as immune killing (*14*, *19*) and the need to wrestle with parameter identifiability issues (*12*, *18*, *20*).

To illustrate our data-driven approach, we used data on the rodent malaria *Plasmodium chabaudi* in laboratory mice. Infected RBCs burst every 24 hours in this species, releasing on average six merozoites (*21*). Applying Eq. 1 therefore requires daily estimates of numbers of infected and uninfected RBCs. We analyzed experimental work on $CD4^+$ T cell–depleted mice (*22*), intact mice infected at a range of starting parasite densities (*23*), and mice treated with a neutralizing antibody that acts to up-regulate immunity (*24*), all infected with the AS clone of *P. chabaudi* [see figs. S2 to S4 and (*25*) for details]. Framing our analysis in ecological terms (*4*, *14*), we contrasted bottom-up processes (analogous to resource availability for free-living organisms) with top-down mechanisms (analogous to control by natural enemies). There are two widely recognized bottom-up controls in malaria dynamics (*3*, *4*, *11*–*13*, *26*–*28*): the availability of susceptible cells, and age-dependent variation in susceptibility of these cells. For example, younger RBCs (reticulocytes, less than 4 days old) are less susceptible to *P. chabaudi* AS infection than are normocytes (*29*). Both RBC availability and age distribution are shaped by infected cell density (because parasites destroy RBCs) and by RBC supply [erythropoiesis and/or splenic retention of uninfected RBCs (*30*)]. Top-down regulatory mechanisms include innate and adaptive immunity provided by effectors ranging from macrophages to strain-specific antibodies (*9*).

We first estimated the time-varying quantities defined above. In both $CD4^+$ T cell–depleted and intact mice, the effective propagation number ($P_{e,t}$) fluctuated considerably over the course of the infection (Fig. 1). This, combined with the fluctuations in susceptible RBC supply, led to variation in the effective reproductive ratio ($R_{e,t}$), typically ranging from 4 to 6 early in the infection to less than 1 later on. The effect of treatments on $P_{e,t}$ and $R_{e,t}$ revealed three broad determinants of within-host malaria dynamics in rodents, as detailed below.

Dose dependence of early innate immunity. Comparing the dynamics of P_e across inoculum sizes in intact mice (Fig. 1) reveals a surprising and conspicuous dose dependence in the early propagation of the parasite: Higher starting numbers

[1]Department of Zoology, Oxford University, Oxford OX1 3PS, UK. [2]Department of Ecology and Evolutionary Biology, Princeton University, Princeton, NJ 08544, USA. [3]Center for Infectious Disease Dynamics, Pennsylvania State University, State College, PA 16802, USA. [4]Department of Animal and Plant Sciences, University of Sheffield, Western Bank, Sheffield S10 2TN, UK. [5]Fogarty International Center, National Institutes of Health, Bethesda, MD 20892, USA.

*To whom correspondence should be addressed. E-mail: charlotte.metcalf@zoo.ox.ac.uk

of parasites resulted in substantially higher effective propagation numbers early in infections (Fig. 2). This curve resembles the type II functional response classically described for predator-prey systems: If the immune response has a "predator" handling time associated with each "prey" caught (i.e., infected RBCs or free merozoites killed) [e.g., (*31*)], the prey death rate per capita will decline as a function of prey numbers. This interpretation is also compatible with innate immunity modeled as drawing on a limited pool of effectors (*32*). Thus, early host defenses [active within 1 to 4 days and thus likely to reflect an arm of innate immunity (*9*)] can retain R_e near 1 for small numbers of parasites (Fig. 1), but if numbers of parasites are above a threshold, this control is overwhelmed. In fact, the upper limit of the range of burst sizes reported for the AS clone (*6*, *21*) is close to the maximum estimate of R_e observed at high doses (Fig. 1), which suggests that for sufficiently high inocula, there is negligible loss of parasites to immunity in the early phase. More effective control at low doses might contribute to the dose dependence of pre-patency observed in human malaria infections during neurosyphilis treatments (*33*). However, detecting dose dependence of innate immune efficacy in human hosts is likely to be complicated, because evidence from both neurosyphilis treatments (*2*, *3*) and vaccine trials (*10*) points to considerable patient-to-patient variability in innate immunity.

Impact of RBC age structure. If adaptive immunity can be assumed to be very impaired in $CD4^+$ T cell–depleted mice (*9*), temporal fluctuations in P_e will primarily reflect the action of RBC availability, age structure, and/or innate immunity. The age structure of RBCs can be inferred via the change in RBC numbers due to processes other than infection of individual cells (*25*) (fig. S5). Major shifts toward younger age classes occurred over the course of the infection: from <5% reticulocytes in uninfected mice to as much as 80% in $CD4^+$ T cell–depleted mice and 40% in intact infected mice (Fig. 1; proportion occupied by gray polygons increases with time). This replacement of normocytes by reticulocytes was associated with a reduction in P_e reflecting reduced average susceptibility of circulating RBCs. We can build on the regression equation defined in Eq. 1 to fit two age-specific propagation parameters (P_{e1} and P_{e2}, which respectively account for effective propagation in normocytes and reticulocytes) to the time series of immune-depleted mice (*25*). Incorporation of these parameters significantly improved the fit to the temporal pattern of effective propagation relative to a model lacking age structure (fig. S7) (likelihood ratio = 11.53, $P < 0.01$, df = 1). This provides direct empirical evidence of the importance of RBC age structure to control of malaria parasites in immune-depleted mice. Indeed, the joint effect of RBC depletion and skewed age structure results in a factor of 3 reduction of the effective reproductive ratio (table S1), which suggests that the many host-dependent mechanisms of RBC reduction that are evident in both rodent

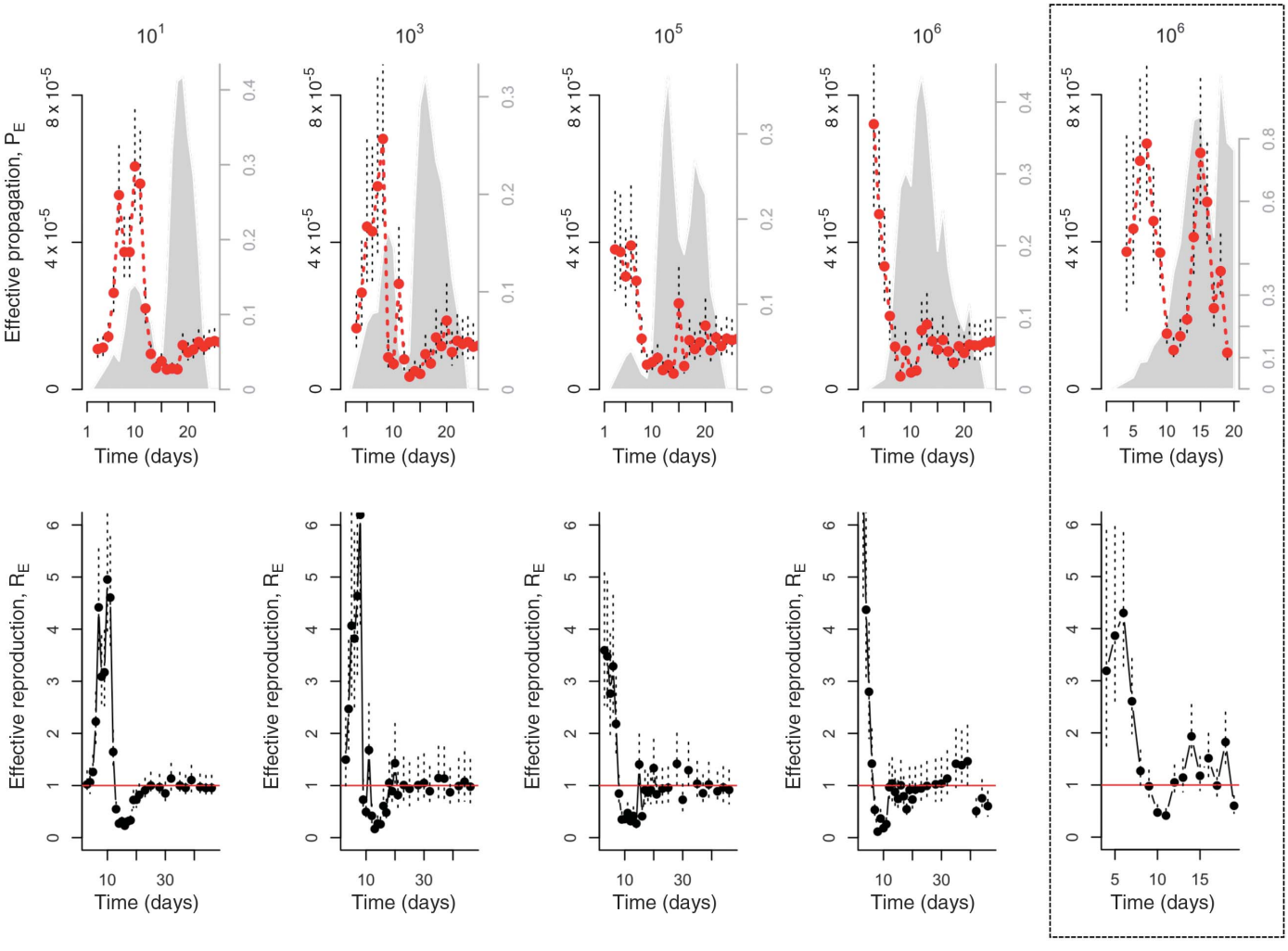

Fig. 1. Within-host effective propagation. The red line is the estimate of effective propagation for 5 or 10 intact AS-infected mice with different inocula sizes (unboxed panels) and five $CD4^+$ T cell–depleted AS-infected mice (boxed panels). The size of the inoculum is indicated at the top of each column (10^1, 10^3, 10^5, and 10^6 $CD4^+$ T cell–depleted mice inocula sizes are comparable to the largest levels used in intact mice); SEs from the regression are shown as dashed vertical lines. Gray polygons show mean approximate proportion of RBCs aged 1 to 3 days, calculated from reconstructions of RBC change (right axis). The bottom row shows the corresponding R_e up to day 50 for intact mice; P_e changes little over the later days.

and human malaria (*30*) may reflect an evolutionary adaptation.

Impact of adaptive immunity. Using the two RBC age-specific parameters estimated from immune-depleted mice (P_{e1} and P_{e2}), we can predict the pattern of effective propagation through time that would be observed if all fluctuations in $P_{e,t}$ were due to bottom-up controls only, and compare this with the observed time series in intact mice to reveal the relative importance of top-down and bottom-up factors through time (figs. S8 and S9). Our approach reveals that this is also highly dependent on initial parasite dose. For mice inoculated with high doses, dynamics for the first ~10 days were adequately explained by RBC availability and age structure, but after that, the effective propagation number was consistently and substantially overpredicted by the bottom-up model (fig. S9). This indicates that potent top-down controls are established after about a week. Mice infected with low parasite density had an additional early overprediction of $P_{e,t}$ because the bottom-up only model does not capture the ability of early–innate immunity to control propagation from low densities (Fig. 2 and figs. S8 and S9). We can extend the model to incorporate early immunity (Fig. 2) by defining early parasite survival to be a function of parasite density that increases toward a plateau, and fitting this to time series of intact mice (*25*) (fig. S10). A combined model of bottom-up and early innate controls can precisely predict the early propagation numbers and course of infection, but not the later propagation numbers (fig. S9). The failures of prediction from this simple model reflect the action of adaptive immunity. Conversely, successes of this restricted model highlight the interval of time over which failure to account for resource limitation as a mechanism of malaria control could impair inference about immunity (fig. S8).

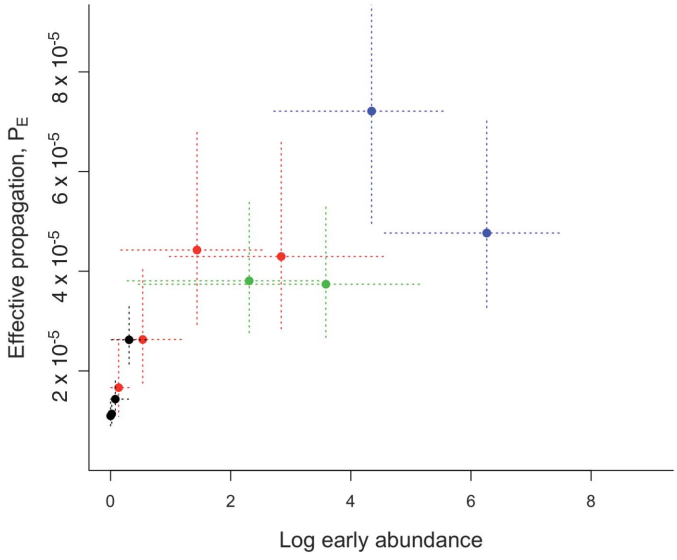

Fig. 2. Decelerating control. Effective propagation over the first 2 to 4 days (with the last day set when $P_{e,t}$ starts to decay sharply; see Fig. 1) for four different starting inoculation sizes: 10^1 in black (n = 10 mice, 3 days), 10^3 in red (n = 5 mice, 4 days), 10^5 in green (n = 5 mice, 2 days), 10^6 in blue (n = 5 mice, 2 days). These results indicate a decelerating function of density suggestive of a handling-time effect for innate immunity. Vertical lines are SEs from the regression defining $P_{e,t}$; horizontal lines are 95% quantiles for abundance of parasites observed on that day.

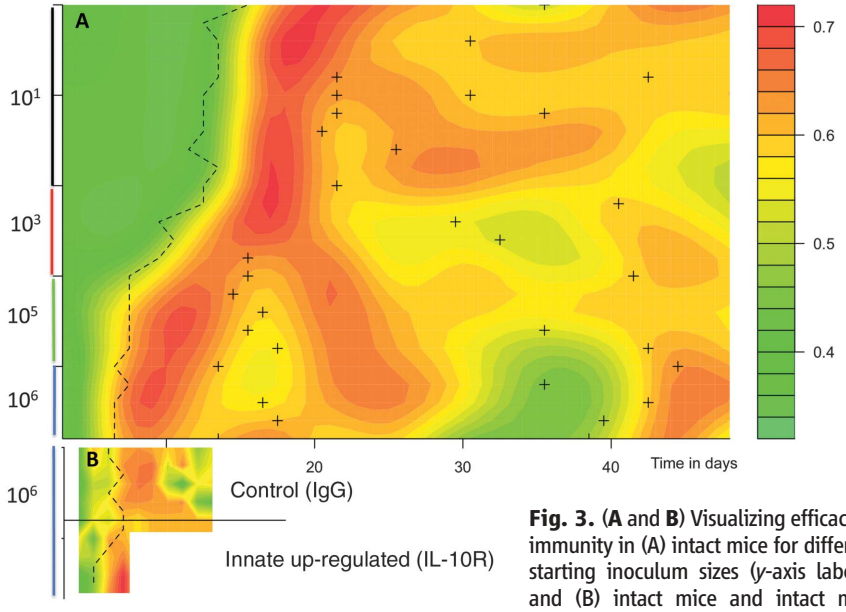

Fig. 3. (**A** and **B**) Visualizing efficacy of immunity in (A) intact mice for different starting inoculum sizes (*y*-axis labels), and (B) intact mice and intact mice treated with IL-10R, which up-regulates innate immunity (*y*-axis labels to the right). Surfaces show smoothed proportion of infected cells killed, p_t, against time in days (*x* axis) with mice ranked via their early densities within each category (rows, *y* axis); dashed thick line indicates the timing of the first major peak of infection; and for (A) the crosses indicate secondary peaks, generally following dips in immune efficacy. In (A), higher early densities experience an earlier increase in mortality of infected cells, but this effect decays, then increases, and finally dips again around day 35 concomitant with a resurgence of parasites. In (B), mice treated with IL-10R experience an earlier peak in immune efficacy. However, treated mice generally die by day 9.

The discrepancy between observed and predicted values of P_e allows us to calculate the efficacy of immune clearance via the proportion of infected cells p_t that must be killed to obtain the observed number of parasitized cells while accounting for RBC limitation (*25*). To visualize changes in immune efficacy (parasite kill rates), we plotted the smoothed surface of this fraction through time, ranking mice by early parasite density (Fig. 3A). Immune efficacy peaks around 0.85, indicating that at its maximum efficacy, adaptive immunity removes on the order of 85% of parasites per day, resulting in a factor of 13 reduction in the effective reproductive ratio (table S1). From an applied point of view, this quantification might represent a useful yardstick against which the efficacy of immunity elicited by candidate vaccines or new drugs could be measured. The peak efficacy was similar in all mice, irrespective of inoculating dose, but the timing of the peak varied. Mice receiving higher doses experienced an earlier peak in parasitemia (Fig. 3A, dashed line) and an earlier increase in immune efficacy (as early as day 8 versus as late as day 20 for the lowest dose; Fig. 3A). Declines in immune efficacy occurred after initial parasitemia was controlled, with kill rates approximately halved (Fig. 3A). This decline—which might reflect down-regulation of immunity (under host or parasite control), depletion of the immune effector pool, and/or antigen escape—allowed the re-emergence of parasitemia in some mice (fig. S3). The pattern of decline was complex and dose-dependent (Fig. 3A). Higher starting densities resulted in a rapid dip in immune efficacy following the initial peak. Subsequently, in response to recrudescence (fig. S3, peaking at around 15 days, fig. S11), immune efficacy increased and then decayed again (around day 35). By contrast, mice infected with intermediate starting densities experienced slower declines in immunity. Feedbacks inherent in activation of adaptive immunity may partly underlie this variability (*34*, *35*): If conditions at the peak of infection are such that few susceptible RBCs are available, control may be achieved by relatively less sustained immune

killing, with the result that immune memory is retained less well (*36*) for higher inoculum sizes.

To further illustrate how the time series approach can provide new insights from manipulative immunological experiments, we calculated surfaces of immune efficacy for control mice and for mice treated with antibodies to interleukin-10 receptor (anti–IL-10R) (Fig. 3B). Treated mice experienced a slightly earlier increase in immune efficacy, in keeping with the accelerated innate response generated by blockade of the potent modulatory cytokine IL-10 (*24*). This slight difference in the timing of peak immune efficacy between anti–IL-10R–treated and untreated mice resulted in rather different maximum parasite densities (Fig. 4A). Two factors may explain this. First, because malaria within-host kinetics are so dynamic, a small impact at the right time may have a large consequence several merozoite generations later. Second, anti–IL-10R–treated mice experienced earlier anemia (Fig. 4A), perhaps attributable to increased bystander killing, suppression of erythropoiesis, and/or retention of uninfected RBCs by the spleen [some of which are likely repercussions of increased tumor necrosis factor–α production (*30*)]. Consequently, there was a decline in the effective reproductive ratio in treated mice, beyond the reduction due to direct killing of infected cells (Fig. 4). Therefore, this immune manipulation generated an apparent increase in immune efficacy (in the sense that the effective propagation number was reduced) that was mediated via a resource depletion mechanism. Low levels of IL-10 have been implicated in severe anemia in human malaria (*37*), which suggests that similar mechanisms could be operating. An intriguing corollary is that substantial bystander killing [whereby more than four uninfected cells may be killed for every infected cell killed during rodent malaria (*4*)], rather than being an unintended side effect of immune activity, may in part be an evolutionary adaptation for using top-down mechanisms to enhance bottom-up controls.

Discussion. Antiparasite effects of RBC resource limitation (e.g., via suppression of erythropoiesis or by the action of protective RBC polymorphisms that reduce susceptibility) are indicated by a range of studies on human malaria (*38*, *39*). A key merit of the effective propagation number is that it provides a straightforward way of controlling for effects of target cell availability on within-host replication, thus revealing the relative and absolute strength of mechanisms that drive within-host dynamics (e.g., killing of infected cells, or heterogeneities among target cells in transmission characteristics) and their variation through time. The method also yields a direct quantification of fluctuations in the within-host effective reproduction number R_e, thus identifying key points for interventions—for example, when parasite effective reproduction is so low that any additional challenge to growth may result in clearance of the infection (*8*), with potential relevance for applications toward human health. Finally, our application of the methodology to the *P. chabaudi* case study shows that the method can reveal previously overlooked aspects of control in mouse malaria, producing new hypotheses for the regulation of human malaria. Interestingly, the diminishing impact of innate immunity with increased dose may be the selective pressure responsible for the evolution of the large burst size of liver schizonts (and, as a consequence, the long incubation period in the liver), which is compatible with estimates of 10^5 to 10^6 merozoites released after a single infective bite (*40*), which is robustly over the threshold of innate immune escape discovered here (Fig. 2).

Previous work on malaria has fitted more mechanistically detailed dynamic models to time-series data on uninfected and infected cells (*3*, *4*, *11*–*14*, *26*, *41*). Our simpler statistical method confirms conclusions from this work [e.g., roles for the age structure of RBCs (*12*, *13*) and for the clearance of uninfected RBCs (*11*)] but also identifies dynamical features not previously detected (e.g., dose dependence in the impact of innate immunity; complex time dependence in the efficacy of adaptive immunity). Our method also sidesteps much of the difficulty involved in fitting such models and provides empirical insights into the shapes that functional forms in more mechanistic models should reflect [such as the dose-dependent saturation of the early innate control (Fig. 2) or the response surface of adaptive immunity (Fig. 3)]. As shown (Fig. 3B and Fig. 4), our approach enables detailed interpretations of existing experimental data [e.g., time series following knockdown of immune factors (*42*, *43*), induced erythropoiesis or blood transfusions (*41*, *44*), etc.]. Given time series of susceptible and infected RBCs, estimates of time-varying effective

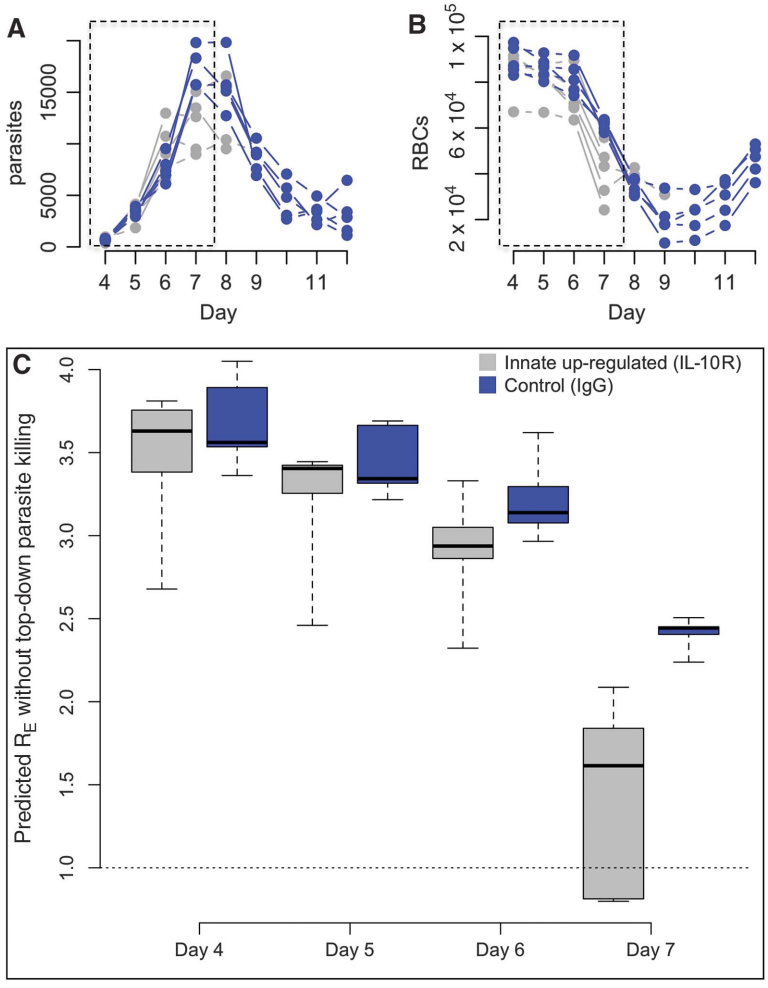

Fig. 4. (**A** and **B**) Top-down controls acting via bottom-up effects. Time series ($\times 10^{-2}$ per μl) of parasites (A) and RBCs (B) for mice treated with IL-10R (gray, $n = 4$) and controls (blue, $n = 4$). (**C**) Corresponding estimates of the effective reproductive ratio R_e on days 4 to 7 that would be observed in the absence of immune killing of infected cells, obtained by combining RBC age-specific estimates of P_e obtained from $CD4^+$ T cell–depleted mice with the RBC dynamics and age structure indicated by these time series. Dashed boxes in (A) and (B) show the time period plotted in (C). In IL-10R–treated mice, this predicted R_e drops precipitously as a result of RBC depletion alone (B); this anemia is not due to parasite levels, which remain comparable in controls and treated mice (A). This indicates that immune-mediated killing of uninfected RBCs is a key mechanism of control.

propagation are directly accessible to anyone with basic statistical knowledge. This should ultimately open the way for a complete characterization of the roles of direct and indirect top-down and bottom-up mechanisms involved in the regulation of parasite densities (fig. S12 and table S1) in the context of both single and mixed infections, and how this in turn affects transmission and disease severity.

The underlying process of bursting infected RBCs and invasion of uninfected RBCs is common to blood-phase malaria across animal taxa. The methods we introduce will consequently be generally applicable. The strength of the mouse data we have used is the finely resolved measures of uninfected and infected red blood cells. We are unaware of any experimental time series in human patients in which these parameters were directly measured, but our analyses suggest that future longitudinal studies of individual patients that undertake the simple assays required to directly assess RBC densities in addition to parasite densities will lead to considerable insights into the factors regulating human malaria.

References and Notes

1. R. Carter, D. Walliker, *Ann. Trop. Med. Parasitol.* **69**, 187 (1975).
2. L. Molineaux, M. Träuble, W. E. Collins, G. M. Jeffery, K. Dietz, *Trans. R. Soc. Trop. Med. Hyg.* **96**, 205 (2002).
3. K. Dietz, G. Raddatz, L. Molineaux, *Am. J. Trop. Med. Hyg.* **75** (suppl.), 46 (2006).
4. D. T. Haydon, L. Matthews, R. Timms, N. Colegrave, *Proc. R. Soc. B* **270**, 289 (2003).
5. R. M. Ribeiro *et al.*, *J. Virol.* **84**, 6096 (2010).
6. O. N. Bjørnstad, B. Finkenstädt, B. T. Grenfell, *Ecol. Monogr.* **72**, 169 (2002).
7. R. M. Anderson, R. M. May, *Infectious Diseases of Humans* (Oxford Univ. Press, Oxford, 1991).
8. M. A. Nowak, R. M. May, *Virus Dynamics: Mathematical Principles of Immunology and Virology* (Oxford Univ. Press, Oxford, 2000).
9. M. M. Stevenson, E. M. Riley, *Nat. Rev. Immunol.* **4**, 169 (2004).
10. M. Walther *et al.*, *J. Immunol.* **177**, 5736 (2006).
11. M. R. Miller, L. Råberg, A. F. Read, N. J. Savill, *PLOS Comput. Biol.* **6**, e1000946 (2010).
12. N. Mideo *et al.*, *Am. Nat.* **172**, E214 (2008).
13. R. Antia, A. Yates, J. C. de Roode, *Proc. R. Soc. B* **275**, 1449 (2008).
14. B. F. Kochin, A. J. Yates, J. C. de Roode, R. Antia, *PLoS ONE* **5**, e10444 (2010).
15. A. Handel, I. M. Longini Jr., R. Antia, *J. R. Soc. Interface* **7**, 35 (2010).
16. C. L. Ball, M. A. Gilchrist, D. Coombs, *Bull. Math. Biol.* **69**, 2361 (2007).
17. A. S. Perelson, *Nat. Rev. Immunol.* **2**, 28 (2002).
18. R. A. Saenz *et al.*, *J. Virol.* **84**, 3974 (2010).
19. K. A. Lythgoe, L. J. Morrison, A. F. Read, J. D. Barry, *Proc. Natl. Acad. Sci. U.S.A.* **104**, 8095 (2007).
20. L. Molineaux, K. Dietz, *Parassitologia* **41**, 221 (1999).
21. R. Killick-Kendrick, W. Peters, Eds., *Rodent Malaria* (Academic Press, London, 1978).
22. V. C. Barclay *et al.*, *Proc. R. Soc. B* **275**, 1171 (2008).
23. S. Huijben, thesis, University of Edinburgh (2010).
24. G. H. Long, B. H. K. Chan, J. E. Allen, A. F. Read, A. L. Graham, *BMC Evol. Biol.* **8**, 128 (2008).
25. See supporting material on *Science* Online.
26. P. G. McQueen, F. E. McKenzie, *Proc. Natl. Acad. Sci. U.S.A.* **101**, 9161 (2004).
27. B. Hellriegel, *Proc. R. Soc. B* **250**, 249 (1992).
28. C. Hetzel, R. M. Anderson, *Parasitology* **113**, 25 (1996).
29. W. Jarra, K. N. Brown, *Parasitology* **99**, 157 (1989).
30. A. A. Lamikanra *et al.*, *Blood* **110**, 18 (2007).
31. S. S. Pilyugin, R. Antia, *Bull. Math. Biol.* **62**, 869 (2000).
32. R. Antia, J. C. Koella, *J. Theor. Biol.* **168**, 141 (1994).
33. J. R. Glynn, D. J. Bradley, *Parasitology* **110**, 7 (1995).
34. M. S. Russell *et al.*, *J. Immunol.* **179**, 211 (2007).
35. D. L. Chao, M. P. Davenport, S. Forrest, A. S. Perelson, *Immunol. Cell Biol.* **82**, 55 (2004).
36. R. Stephens, J. Langhorne, *PLoS Pathog.* **6**, e1001208 (2010).
37. C. Othoro *et al.*, *J. Infect. Dis.* **179**, 279 (1999).
38. F. P. Mockenhaupt *et al.*, *Blood* **104**, 2003 (2004).
39. S. Wambua, J. Mwacharo, S. Uyoga, A. Macharia, T. N. Williams, *Br. J. Haematol.* **133**, 206 (2006).
40. K. Baer, C. Klotz, S. H. Kappe, T. Schnieder, U. Frevert, *PLoS Pathog.* **3**, e171 (2007).
41. N. J. Savill, W. Chadwick, S. E. Reece, *PLOS Comput. Biol.* **5**, e1000416 (2009).
42. Z. Su, A. Fortin, P. Gros, M. M. Stevenson, *J. Infect. Dis.* **186**, 1321 (2002).
43. G. H. Long, B. H. K. Chan, J. E. Allen, A. F. Read, A. L. Graham, *Parasitology* **133**, 673 (2006).
44. K.-H. Chang, M. Tam, M. M. Stevenson, *J. Infect. Dis.* **189**, 735 (2004).

Acknowledgments: Our empirical work was funded by the Wellcome Trust (A.F.R., V.C.B., G.H.L.), the Darwin Trust of the University of Edinburgh (S.H.), and the UK Biotechnology and Biological Sciences Research Council (A.L.G., G.H.L.), and the theoretical work by the Bill and Melinda Gates Foundation (C.J.E.M., B.T.G., O.N.B.), the RAPIDD program of the Science and Technology Directorate (B.T.G., A.L.G., A.F.R.), and National Institute of General Medical Sciences grant R01GM089932 (B.G., O.N.B., A.F.R.). We thank N. Mideo and P. Klepac for extensive discussion. All authors discussed the results and implications and commented on the manuscript at all stages. C.J.E.M. and O.N.B. developed the statistical approach; A.F.R., V.B., and S.H. designed and performed the dose-dependent and $CD4^+$ T cell–depleted mice experiments; A.L.G. and G.H.L. designed and performed the innate immunity experiments. The authors declare no competing interests.

Supporting Online Material

www.sciencemag.org/cgi/content/full/333/6045/984/DC1
Materials and Methods
SOM Text
Figs. S1 to S12
Table S1
References

21 February 2011; accepted 22 June 2011
10.1126/science.1204588

A Large and Persistent Carbon Sink in the World's Forests

Yude Pan,[1]* Richard A. Birdsey,[1] Jingyun Fang,[2,3] Richard Houghton,[4] Pekka E. Kauppi,[5] Werner A. Kurz,[6] Oliver L. Phillips,[7] Anatoly Shvidenko,[8] Simon L. Lewis,[7] Josep G. Canadell,[9] Philippe Ciais,[10] Robert B. Jackson,[11] Stephen W. Pacala,[12] A. David McGuire,[13] Shilong Piao,[2] Aapo Rautiainen,[5] Stephen Sitch,[7] Daniel Hayes[14]

The terrestrial carbon sink has been large in recent decades, but its size and location remain uncertain. Using forest inventory data and long-term ecosystem carbon studies, we estimate a total forest sink of 2.4 ± 0.4 petagrams of carbon per year (Pg C $year^{-1}$) globally for 1990 to 2007. We also estimate a source of 1.3 ± 0.7 Pg C $year^{-1}$ from tropical land-use change, consisting of a gross tropical deforestation emission of 2.9 ± 0.5 Pg C $year^{-1}$ partially compensated by a carbon sink in tropical forest regrowth of 1.6 ± 0.5 Pg C $year^{-1}$. Together, the fluxes comprise a net global forest sink of 1.1 ± 0.8 Pg C $year^{-1}$, with tropical estimates having the largest uncertainties. Our total forest sink estimate is equivalent in magnitude to the terrestrial sink deduced from fossil fuel emissions and land-use change sources minus ocean and atmospheric sinks.

Forests have an important role in the global carbon cycle and are valued globally for the services they provide to society. International negotiations to limit greenhouse gases require an understanding of the current and potential future role of forest C emissions and sequestration in both managed and unmanaged forests. Estimates by the Intergovernmental Panel on Climate Change (IPCC) show that the net uptake by terrestrial ecosystems ranges from less than 1.0 to as much as 2.6 Pg C $year^{-1}$ for the 1990s (*1*). More recent global C analyses have estimated a terrestrial C sink in the range of 2.0 to 3.4 Pg C $year^{-1}$ on the basis of atmospheric CO_2 observations and inverse modeling, as well as land observations (*2*–*4*). Because of this uncertainty and the possible change in magnitude over time, constraining these estimates is critically important to support future climate mitigation actions.

[1]U.S. Department of Agriculture Forest Service, Newtown Square, PA 19073, USA. [2]Key Laboratory for Earth Surface Processes, Ministry of Education, Peking University, Beijing, 100871 China. [3]State Key Laboratory of Vegetation and Environmental Change, Institute of Botany, Chinese Academy of Sciences, Beijing, 100093 China. [4]Woods Hole Research Center, Falmouth, MA 02543, USA. [5]University of Helsinki, Helsinki, Finland. [6]Natural Resources Canada, Canadian Forest Service, Victoria, BC, V8Z 1M5, Canada. [7]School of Geography, University of Leeds, LS2 9JT, UK. [8]International Institute for Applied Systems Analysis, Laxenburg, Austria. [9]Global Carbon Project, Commonwealth Scientific and Industrial Research Organization Marine and Atmospheric Research, Canberra, Australia. [10]Laboratoire des Sciences du Climat et de l'Environnement CEA-UVSQ-CNRS, Gif sur Yvette, France. [11]Duke University, Durham, NC 27708, USA. [12]Princeton University, Princeton, NJ 08544, USA. [13]U.S. Geological Survey, Alaska Cooperative Fish and Wildlife Research Unit, University of Alaska, Fairbanks, AK 99775, USA. [14]Oak Ridge National Laboratory, Oak Ridge, TN 37831, USA.

*To whom correspondence should be addressed. E-mail: ypan@fs.fed.us